Activation of O_2 and CO_2 by PtO^+: The Thermochemistry of PtO_2^+

Xiao-Guang Zhang and P. B. Armentrout*

Department of Chemistry, University of Utah, Salt Lake City, Utah 84112-0850

Received: July 12, 2003; In Final Form: August 22, 2003

Reactions of PtO^+ with O_2 and CO_2 and the collision-induced dissociation of PtO^+ with Xe and of PtO_2^+ with Xe and Ar have been studied as a function of kinetic energy using guided ion beam tandem mass spectrometry in order to elucidate the thermochemistry of PtO_2^+. The kinetic energy dependences for these reactions show endothermic behavior except for $Pt^+{\cdot}O_2 + Xe \rightarrow PtXe^+ + O_2$. Analyses of the endothermic reaction cross sections yield the 0 K bond dissociation energies (BDEs) in eV (kJ/mol) of $D_0(OPt^+-O) = 3.06 \pm 0.07$ (295 ± 7), $D_0(Pt^+-O_2) = 0.67 \pm 0.05$ (65 ± 5), $D_0(OPt^+-CO) = 2.21 \pm 0.10$ (213 ± 10), $D_0(OCPt^+-O) = 3.21 \pm 0.12$ (310 ± 12), and $D_0(Pt^+-Ar) = 0.34 \pm 0.09$ (29 ± 9), reasonably consistent with available theoretical values. Combining the OPt^+-O BDE measured here with literature data also yields the ionization energy of OPtO as 10.56 ± 0.48 eV. These data, along with complementary ab initio calculations, enable the potential energy surfaces for the activation of O_2 by Pt^+ to be mapped out in some detail. Evidence is presented that PtO_2^+ has stable structures of both $O-Pt^+-O$ and $Pt^+{\cdot}O_2$.

1. Introduction

In the preceding paper,[1] a case is made for an interest in understanding the energetics and reactivity of platinum oxides. Platinum is an active component of versatile catalysts, e.g., for the oxidation of CO and unburned hydrocarbons in the control of car emissions.[2,3] The intrinsic reactivity of such species can be examined in the gas phase where supports and solvent interactions are absent.

Previously we have used guided ion beam tandem mass spectrometry to study the metal dioxides, MO_2^+, of the first-row[4,5] and second-row[4,6,7,8,9] transition metal ions, and other metal ions.[4] In the present work, we extend these studies to the third-row transition metal ion, platinum. Recently Schwarz's group used ion cyclotron resonance (ICR) mass spectrometry, various theoretical calculations, and preliminary experimental values from our work as anchors to study the energetics and reactivities of the PtO_2^+ species.[10] However, the ICR experiments were performed at thermal energy, whereas the use of guided ion beam tandem mass spectrometry allows the examination of the kinetic energy dependence of both exothermic and endothermic processes. Analysis of such data provides experimental bond dissociation energies (BDEs) that can be used as benchmarks for comparison with theoretical models of the structure and bonding of PtO_2^+. Furthermore, PtO_2^+ has been shown to activate and oxygenate hydrocarbons,[10−13] making it a potentially useful model of systems that can transform hydrocarbons into other useful chemicals. The present work provides thermodynamic, dynamic, and mechanistic information for the activation of O_2 and CO_2 by PtO^+. The dynamics of such ion−molecule reactions and the related thermochemistry are of obvious fundamental interest and have implications in understanding a variety of catalytic reactions involving transition metal systems.[14−16]

2. Experimental Section

2.1. General Procedures. The guided ion beam tandem mass spectrometer on which these experiments were performed has been described in detail previously.[17,18] Details of the present experiments are described fully in the preceding paper.[1]

PtO^+ ions are produced through reaction of Pt^+ with N_2O. PtO_2^+ ions are produced by sequential reactions of Pt^+ with N_2O in the DC/FT source and by the three-body condensation of Pt^+ with O_2 in the DC/FT source. In those cases, the reactant gas (N_2O or O_2) is introduced into the flow tube 30 cm downstream of the discharge zone at a pressure of ~2 mTorr. These ions undergo $\sim 10^5$ thermalizing collisions with He and $\sim 10^4$ collisions with Ar along the flow tube before entering the guided ion beam apparatus. These collisions with the He/Ar flow gas stabilize and thermalize the ions both rotationally and vibrationally. We assume that these ions are in their ground electronic state and that the internal energy of these molecular ions is well described by a Maxwell−Boltzmann distribution of rotational and vibrational states corresponding to 300 K, the temperature of the flow tube. Previous studies from this laboratory have shown that these assumptions are consistent with the production of thermalized molecular ions under similar conditions.[14−16,19−21] However, as discussed in the preceding paper,[1] there are probably small amounts of excited states in the PtO^+ beam produced here, as evidenced in the ligand exchange reaction with CO. The possible influence that such states may have on the systems examined here will be carefully evaluated.

2.2. Data Analysis. The kinetic energy dependence of product cross sections is analyzed as detailed in the preceding paper.[1] To determine E_0, endothermic reaction cross sections are modeled using eq 1,[19,22−24]

$$\sigma(E) = \sigma_0 \sum g_i (E + E_i - E_0)^n / E \qquad (1)$$

where σ_0 is an energy-independent scaling factor, E is the relative kinetic energy of the reactants, and n is an adjustable parameter. The sum considers contributions from rovibrational states of the reactants at 300 K, denoted by i, having energies E_i and populations g_i, where $\sum g_i = 1$. The various sets of vibrational frequencies and rotational constants used to determine E_i in this work are taken from the literature for O_2,[25] CO_2,[26] PtO^+,[10,27] $OPtO^+$,[10] and PtO_2^+.[10] Before comparison with the

* Corresponding author. E-mail: armentrout@chem.utah.edu.

10.1021/jp036015b CCC: $25.00
Published on Web 09/30/2003

experimental data, eq 1 is convoluted with the kinetic energy distributions of the reactant ions and neutral reactants at 300 K. The σ_0, n, and E_0 parameters are then optimized using a nonlinear least-squares analysis to give the best reproduction of the data.[28] Error limits for E_0 are calculated from the range of threshold values for different data sets over a range of acceptable n values combined with the absolute uncertainties in the kinetic energy scale and internal energies of the reactant ions.

At higher energies, the cross sections decline because the product ions have sufficient energy to dissociate. In this high-energy region, the data can be modeled by modifying eq 1 to include the dissociation probability according to a statistical model discussed elsewhere.[29] This probability is controlled by two parameters: p, which is an adjustable parameter similar to n, and E_d, which is the energy at which product ions start decomposing. In this study, the values of p and E_d are allowed to vary (although p can only hold integral values) and used to fit cross sections of PtO^+ with O_2 and CO_2, and PtO_2^+ with Ar. Use of this high-energy model does not alter significantly the analysis of the threshold regions.

2.3. Theoretical Calculations. To establish the character of the molecular orbitals of the platinum oxides and to elucidate the potential energy surface for the PtO_2^+ system, quantum chemistry calculations were computed with the B3LYP hybrid density functional method,[30,31] and performed with the GAUSSIAN 98 suite of programs.[32] The B3LYP functional is based on the hybrid gradient-corrected exchange functional proposed by Becke[49] combined with the gradient-corrected correlation functional of Lee, Yang, and Parr.[50] The 60 core electrons of platinum are described using a basis set for Pt as described by Ohanessian et al.,[33] which is based on the relativistic effective core potentials (ECP) of Hay-Wadt (HW),[34] equivalent to the Los Alamos ECP (LANL2DZ) basis set. Whereas the HW-ECP is optimized for neutral atoms, the altered basis set of Ohanessian et al. accounts for differential contraction of the *s* orbitals compared to the *d* orbitals induced by the positive charge. Calculations of potential energy surfaces (relaxed potential energy scans) were conducted using a 6-31+G(2d) basis set for oxygen, whereas the triple-ζ basis, 6-311+G(3df), was used to characterize all stationary points on these potential energy surfaces. Frequency calculations at this level verified the character of all stationary points. In all cases, the thermochemistry calculated here is corrected for zero-point energy effects after scaling the vibrational frequencies by 0.9804.[35] As a point of comparison, the triple-ζ basis set yields an O_2 bond energy of 5.279 eV compared to the experimental value of 5.115 eV.[25]

3. Experimental Results

3.1. CID of PtO^+ with Xe. To help characterize the PtO^+ reactant, cross sections for the interaction of PtO^+ with Xe were measured and are shown in Figure 1. The products observed correspond to reaction 2, a simple collision-induced dissociation process, and reacction 3, a ligand exchange process.

$$PtO^+ + Xe \rightarrow Pt^+ + O + Xe \quad (2)$$

$$\rightarrow PtXe^+ + O \quad (3)$$

The dominant product channel is reaction 2. Formation of $PtXe^+$ has a slightly lower threshold than that of Pt^+, and peaks around the threshold region for reaction 2, indicating that the $PtXe^+$ product decomposes to $Pt^+ + Xe$ at higher energies.

The cross section data for reaction 2 are analyzed using eq 1, and the fitting parameters obtained are listed in Table 1. The model reproduces the experimental data up to ~9 eV with a threshold of 3.78 ± 0.05 eV. The threshold for CID can equal the Pt^+-O BDE as long as the interaction of Pt^+ with O is attractive everywhere, i.e., there are no barriers in excess of the asymptotic dissociation energy, and the dissociation produces ground-state Pt^+ and O products. The former condition is almost certainly true here because the potential for interaction of $Pt^+ + O$ should be attractive at both long-range and short-range.[14,19,23,36] The latter condition is generally true when the dissociation pathway conserves spin, as it does here for $PtO^+(^4\Sigma^-) \rightarrow Pt^+(^2D) + O(^3P)$. For strongly bound species with few internal degrees of freedom, CID experiments may only measure an upper limit for the thermodynamic BDE because of inefficiencies in the transfer of kinetic to internal energy in the collision process.[20,37] This appears to be the case here as the CID threshold of 3.78 ± 0.05 eV exceeds $D_0(Pt^+-O) = 3.26 \pm 0.07$ eV, as measured in the preceding paper.[1] Models in which the threshold energy was held to a value of 3.26 eV did not reproduce the data satisfactorily.

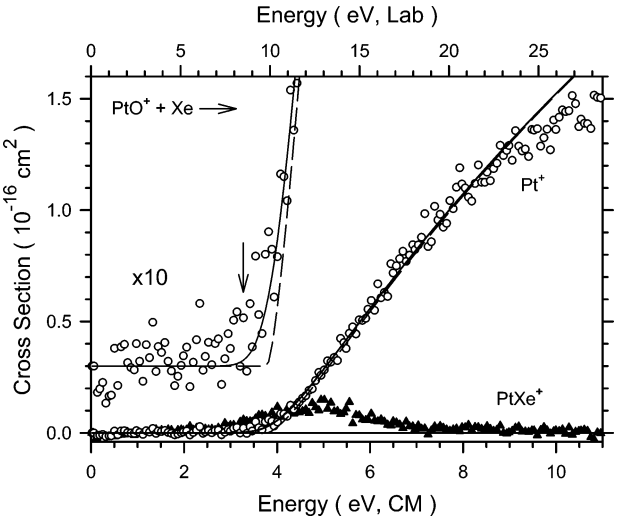

Figure 1. Cross sections for collision-induced dissociation and ligand exchange of PtO^+ with Xe (extrapolated to zero pressure) as a function of kinetic energy in the center-of-mass frame (lower axis) and laboratory frame (upper axis). The best fit to the Pt^+ data (open circles) using eq 1 with parameters in Table 1 is shown as a dashed line. The solid line shows this model convoluted over the kinetic and internal energy distributions of the neutral reactant and ion. The arrow indicates the bond energy E_0 for production of Pt^+ measured in the preceding paper.[1]

TABLE 1: Parameters of Eq 1 Used in Modeling Various Reaction Systems

reactants	products	σ_0	n	E_0 (eV)
$PtO^+ + Xe$	$Pt^+ + O + Xe$	1.0 ± 0.1	1.5 ± 0.1	3.78 ± 0.05
$PtO^+ + O_2$	$PtO_2^+ + O$	0.6 ± 0.1	1.9 ± 0.1	2.04 ± 0.05
	$Pt^+ + O + O_2$	1.9 ± 0.4	1.4 ± 0.1	3.50 ± 0.12
$PtO^+ + CO_2$	$PtO_2^+ + CO$	0.05 ± 0.01	1.7 ± 0.1	2.40 ± 0.05
	$PtCO_2^+ + O$	0.05 ± 0.01	1.6 ± 0.1	3.24 ± 0.10
	$Pt^+ + O + CO_2$	0.5 ± 0.1	1.7 ± 0.1	3.63 ± 0.05
$PtO_2^+ + Xe$	$Pt^+ + O_2 + Xe$	5.4 ± 0.1	1.6 ± 0.1	0.79 ± 0.05
$PtO_2^+ + Ar$	$Pt^+ + O_2 + Ar$	3.4 ± 0.1	1.9 ± 0.1	0.67 ± 0.05
	$PtAr^+ + O_2$	5.9 ± 0.1	1.7 ± 0.1	0.29 ± 0.05
$OPtO^+ + Xe$	$Pt^+ + O_2 + Xe$	0.2 ± 0.1	1.9 ± 0.1	1.19 ± 0.10
	$PtO^+ + O + Xe$	1.0 ± 0.1	1.7 ± 0.1	3.36 ± 0.10

3.2. Reactions of PtO^+ with O_2. Cross sections for the reaction of PtO^+ with O_2 are shown in Figure 2. The products observed correspond to the endothermic reactions 4 and 5.

$$PtO^+ + O_2 \rightarrow PtO_2^+ + O \quad (4)$$

$$\rightarrow Pt^+ + O_2 + O \quad (5)$$

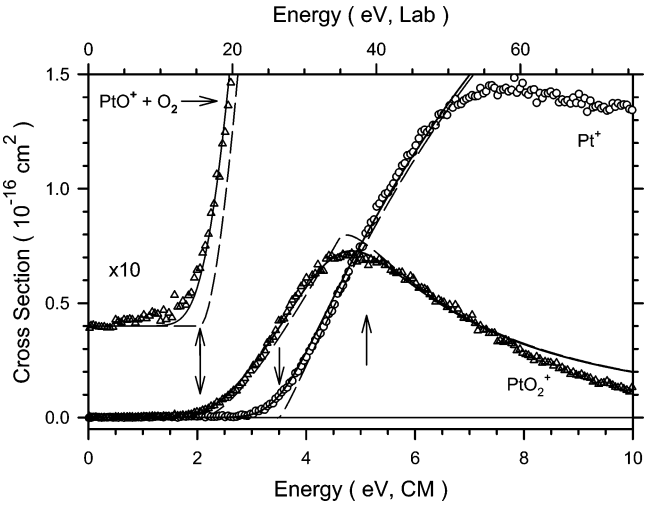

Figure 2. Cross sections for reactions of PtO^+ with O_2 as a function of kinetic energy in the center-of-mass frame (lower axis) and laboratory frame (upper axis). The best fits to the data using eq 1 with parameters in Table 1 are shown as dashed lines. The solid lines show these models convoluted over the kinetic and internal energy distributions of the neutral reactant and ion. A high energy model for the PtO_2^+ channel considers dissociation beginning at 4.60 eV, see text. The arrows indicate the threshold energies E_0 and $D_0(O-O)$ at 5.12 eV.

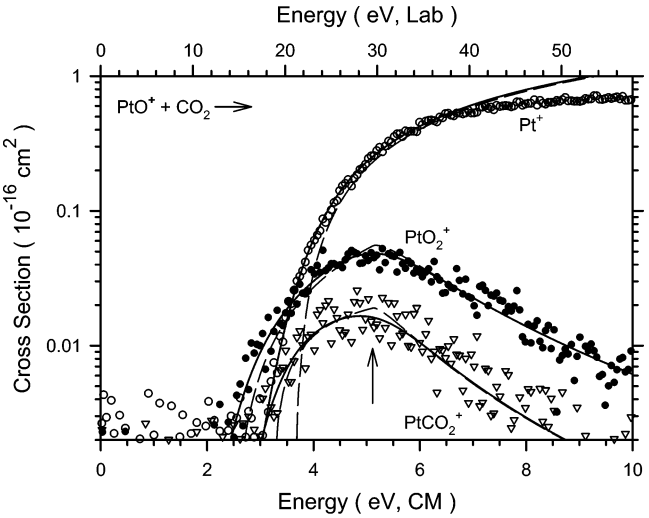

Figure 3. Cross sections for reactions of PtO^+ with CO_2 as a function of kinetic energy in the center-of-mass frame (lower axis) and laboratory frame (upper axis). The best fits to the data using eq 1 with parameters in Table 1 are shown as dashed lines. The solid lines show these models convoluted over the kinetic and internal energy distributions of the neutral reactant and ion. A high energy model for the PtO_2^+ and $PtCO_2^+$ channels considers the dissociation beginning at 5.45 eV. The arrow indicates $D_0(O-CO)$ at 5.45 eV.

This latter reaction can be viewed as a simple collision-induced dissociation process, but can also occur by expulsion of O_2 from the PtO_2^+ product. At lower energies, reaction 4 is the main product channel; however, the cross section decreases at higher energies because PtO_2^+ may be formed with an internal energy in excess of its dissociation energy. Dissociation can conceivably occur by O_2 elimination, reaction 5, or can begin at the bond energy of O_2 (5.12 eV), leading to the overall reaction 6.

$$PtO^+ + O_2 \rightarrow PtO_2^+ + O \rightarrow PtO^+ + O + O \qquad (6)$$

The cross section data are analyzed using eq 1 and the fitting parameters obtained are listed in Table 1. The Pt^+ cross sections are reproduced up to ~6.5 eV. The PtO_2^+ cross sections can be reproduced up to 7 eV with $p = 2$ and an apparent dissociation energy of $E_d \sim 4.6$ eV, well above the onset for dissociation to $Pt^+ + O_2$, which can begin at 3.26 eV = $D_0(Pt^+-O)$. This value of E_d is apparently lower than $D_0(O_2)$ because of the competition with reaction 5 above ~3.5 eV, which dominates the products at higher energies. There is a small tail in the PtO_2^+ cross section at low energies (visible in the expansion of the data, Figure 2) that probably results from trace amounts of excited states of the PtO^+ reactant, as identified in the previous paper[1] and discussed further below.

3.3. Reactions of PtO^+ with CO_2. PtO^+ reacts with CO_2 to form three ionic products in reactions 7, 8, and 9 as shown in Figure 3.

$$PtO^+ + CO_2 \rightarrow Pt^+ + O + CO_2 \qquad (7a)$$

$$\rightarrow Pt^+ + O_2 + CO \qquad (7b)$$

$$\rightarrow PtO_2^+ + CO \qquad (8)$$

$$\rightarrow PtCO_2^+ + O \qquad (9)$$

$PtCO^+$ is also observed but has a maximum cross section below 5×10^{-19} cm^2, and as a consequence is not shown here because it is very noisy. Reaction 7a is a simple collision-induced dissociation process that can begin at 3.26 eV = $D_0(Pt^+-O)$, whereas reaction 7b can begin at 3.60 eV. Reaction 8 appears below the threshold of reaction 7. Its cross section decreases at ~5.5 eV because PtO_2^+ may be formed with an internal energy in excess of the OPt^+-O bond dissociation energy. Overall, this dissociation can begin at the bond energy of CO_2 (5.45 eV), leading to the overall reaction 10.

$$PtO^+ + CO_2 \rightarrow PtO_2^+ + CO \rightarrow PtO^+ + O + CO \qquad (10)$$

In fact, the cross section reaches a maximum slightly before $D_0(OC-O) = 5.45$ eV (see Figure 3), which suggests that competition with reaction 7a or dissociation to $Pt^+ + O_2$, reaction 7b, may influence its shape. Reaction 9 could be a ligand exchange reaction but its energy dependence is similar to reaction 8, suggesting that the product could have a OPt^+-CO structure, a hypothesis discussed further below.

The cross section data for all three processes are analyzed using eq 1, and the fitting parameters obtained are listed in Table 1. The Pt^+ cross section is reproduced up to ~7 eV. The PtO_2^+ cross section can be reproduced up to 10 eV with $p = 3$ and the bond dissociation energy of CO_2 at 5.45 eV. The $PtCO_2^+$ cross section can also be reproduced up to 8 eV with $p = 2$ and $E_d = 5.45$ eV.

3.4. CID of $Pt(O_2)^+$ with Xe and Ar. Cross sections for the interaction of a rare gas, Xe or Ar, with PtO_2^+ formed by three-body condensation of Pt^+ with O_2 in the DC/FT source are shown in Figures 4 and 5. The products observed correspond to reactions 11 and 12.

$$PtO_2^+ + Rg \rightarrow Pt^+ + O_2 + Rg \qquad (11)$$

$$\rightarrow PtRg^+ + O_2 \qquad (12)$$

For both rare gases, formation of PtO^+ was also looked for but not observed, indicating it has a cross section smaller than about 10^{-17} cm^2. For the Xe system, the ligand exchange reaction 12 is exothermic, indicating that the BDE of $PtXe^+$ is higher than that of Pt^+-O_2. Thus, the shape of the Pt^+ cross section for reaction 11 may be strongly influenced by competition with

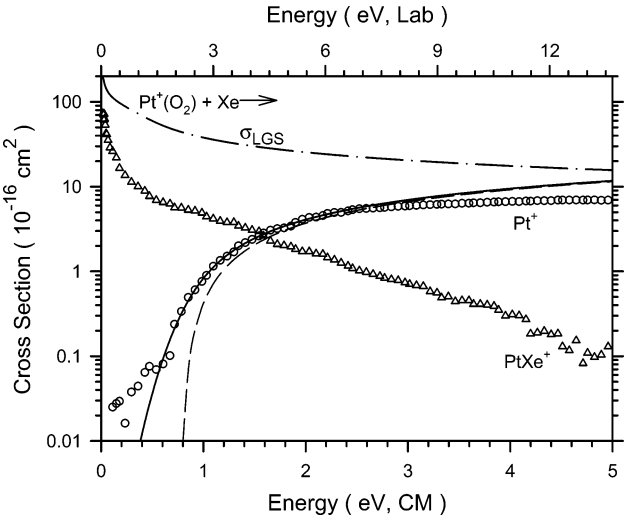

Figure 4. Cross sections for reaction of $Pt^+ \cdot O_2$ (formed by three-body condensation of Pt^+ and O_2) with Xe (extrapolated to zero pressure) as a function of kinetic energy in the center-of-mass frame (lower axis) and laboratory frame (upper axis). The dash−dot line shows the Langevin-Gioumousis-Stevenson (LGS) collision cross section. The best fit to the Pt^+ data (open circles) using eq 1 with parameters in Table 1 is shown as a dashed line. The solid line shows this model convoluted over the kinetic and internal energy distributions of the neutral reactant and ion.

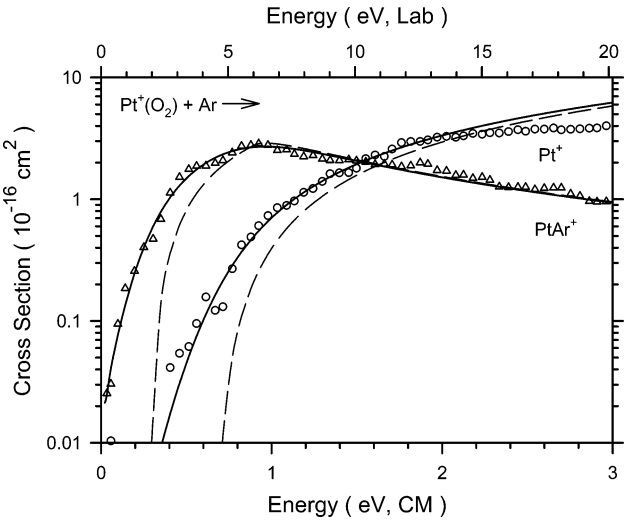

Figure 5. Cross sections for reaction of $Pt^+ \cdot O_2$ (formed by three-body condensation of Pt^+ and O_2) with Ar (extrapolated to zero pressure) as a function of kinetic energy in the center-of-mass frame (lower axis) and laboratory frame (upper axis). The best fits to the data using eq 1 with parameters in Table 1 are shown as dashed lines. The solid lines show these models convoluted over the kinetic and internal energy distributions of the neutral reactant and ion.

the ligand exchange process.[38,39] For the Ar system, the smaller BDE for Pt^+-Ar makes the ligand exchange reaction 12 endothermic. Because there is less competition between these reactions in the Ar system, the threshold for the CID process should be more accurate. The cross section data for the two systems are analyzed using eq 1 and the fitting parameters obtained are listed in Table 1. For the Xe system, the exothermic ligand exchange reaction 12 reaches a reaction efficiency of 38 ± 10% at the lowest energies in comparison with the LGS collision cross section. For the Ar system, the ligand exchange reaction 12 is endothermic and the model of eq 1 reproduces this cross section up to ~3 eV with $p = 1$ and $E_d = 0.90$ eV.

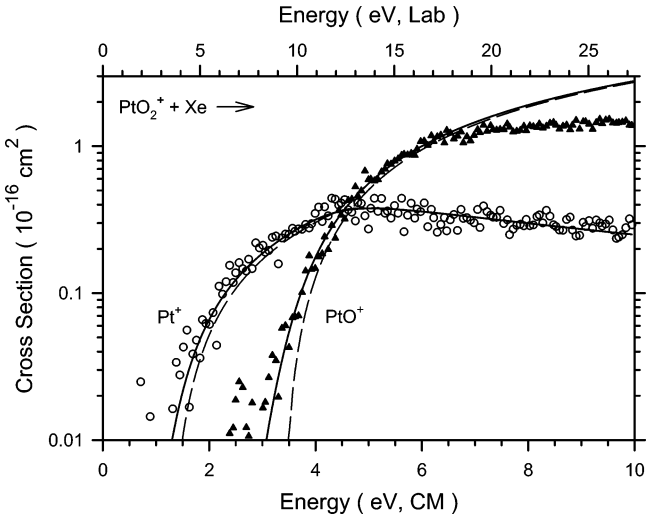

Figure 6. Cross sections for reaction of $OPtO^+$ (formed by sequential reactions of Pt^+ and N_2O) with Xe (extrapolated to zero pressure) as a function of kinetic energy in the center-of-mass frame (lower axis) and laboratory frame (upper axis). The best fits to the Pt^+ (open circles) and PtO^+ (closed triangles) cross sections using eq 1 with parameters in Table 1 are shown as dashed lines. The solid lines show these models convoluted over the kinetic and internal energy distributions of the neutral reactant and ion.

3.5. CID of $OPtO^+$ with Xe. Cross sections for the interaction of Xe with PtO_2^+ formed by sequential reactions of Pt^+ with N_2O in the DC/FT source are shown in Figure 6. The products observed correspond to reactions 13 and 14.

$$OPtO^+ + Xe \rightarrow Pt^+ + O_2 + Xe \quad (13)$$

$$\rightarrow PtO^+ + O + Xe \quad (14)$$

The observation of an intense PtO^+ product is in sharp contrast with the results for $Pt^+ \cdot O_2$, Figures 4 and 5. Further, compared with the cross sections for reaction 11, the Pt^+ cross section here rises more slowly from a higher threshold energy and reaches a magnitude that is an order of magnitude smaller. The shape of the Pt^+ cross section above 4 eV also clearly shows the effects of competition with reaction 14. Small amounts of $PtXe^+$ (maximum of about 0.05 Å^2 from 2 to 4 eV) and $OPtXe^+$ (maximum of about 0.1 Å^2 near 5 eV) were also observed but their cross sections are not shown for clarity. The cross section data for both reactions 13 and 14 are analyzed using eq 1, and the fitting parameters obtained are listed in Table 1. For the CID process, the model of eq 1 reproduces this cross section up to 10 eV with $p = 1$ and $E_d = 4.4$ eV.

4. Thermochemical Results

The endothermic cross-sections in each reaction system are analyzed in detail using eq 1. The optimum values of parameters of this equation are listed for each system in Table 1. Because the rotational, vibrational, and translational energy distributions of reactants are explicitly included in the modeling, the E_0 thresholds determined using eq 1 correspond to 0 K. From the thresholds measured, the BDEs at 0 K for the platinum oxide−ligand product ions observed in the reaction of $PtO^+ + L-R$ to form $OPtL^+ + R$ can be calculated using eq 15

$$D_0(OPt^+ - L) = D_0(L - R) - E_0 \quad (15)$$

where the $D_0(L-R)$ values needed are given in Table 1 of the preceding paper.[1] For collision-induced dissociation (CID), the

TABLE 2: Bond Dissociation Energies at 0 K

	bond energy (eV)[a]		
		theory	
bond	experiment	literature	this work
Pt^+-O	3.26 ± 0.07[b]	3.09,[c,d] 2.96,[c,d] 2.95,[c,d] 2.92[c,d]	2.78[b,d]
OPt^+-O	3.06 ± 0.07, 4.1 ± 0.4[e]	2.85,[c] 2.76,[c] 3.50,[c] 3.62[c]	2.64
Pt^+-O_2	0.67 ± 0.05	0.65,[c,d] 0.65,[c,d] 0.77,[c,d] 0.89[c,d]	0.52[d]
OPt^+-CO	2.21 ± 0.10		1.90
$(CO)Pt^+-O$	3.21 ± 0.12		2.41
Pt^+-Ar	0.34 ± 0.09		
Pt^+-Xe	0.86 ± 0.30[f]		

[a] This work except as noted. [b] Reference 1. [c] Reference 10. [d] A correction of 0.418 eV for the Pt^+ spin−orbit asymptote is made. See text. [e] References 40 and 41. [f] References 20 and 21.

threshold can correspond directly to the BDE for the broken bond. For both bimolecular reactions and CID, we assume that there are no activation barriers in excess of the endothermicity of the reaction, an assumption that is often true for ion−molecule reactions because of the strong long-range attractive forces.[14,19,23,36]

4.1. CID of PtO^+. CID experiments of Pt^+-O with Xe, O_2, and CO_2 yield thresholds of 3.78 ± 0.05 eV, 3.50 ± 0.12 eV, and 3.63 ± 0.05 eV, respectively. Conservatively, these CID thresholds should be viewed as upper limits to the Pt^+-O BDE. We often have found that CID experiments of strongly bound species with few internal degrees of freedom provide thresholds that are higher than the thermodynamic bond energies probably because of inefficiencies in the transfer of kinetic to internal energy in the collision process.[20,37] This appears to be the case here as the CID thresholds all exceed the Pt^+-O BDE of 3.26 ± 0.07 eV determined in the preceding paper.[1] Note, however, that such elevated thresholds are inconsistent with PtO^+ ions that have appreciable internal excitation, as this would lower the observed threshold below the thermodynamic one. This observation means that the observation of excited PtO^+ ions in the preceding paper (reaction of PtO^+ with CO) truly involves a small population of such species.

4.2. OPt^+-O. PtO_2^+ is formed in the reaction of PtO^+ with O_2 and CO_2. The bond dissociation energy $D_0(OPt^+-O)$ is determined to be 3.08 ± 0.05 eV and 3.05 ± 0.05 eV, respectively. This bond energy can also be determined from the threshold for reaction 13, which equals $D_0(Pt^+-O_2)$, because $D_0(OPt^+-O) = D_0(Pt^+-O_2) + D_0(O_2) - D_0(Pt^+-O) = 3.05 \pm 0.12$ eV where the latter two bond energies are taken from ref 1. The weighted average of these three values is 3.06 ± 0.07 eV (where the uncertainty is two standard deviations of the mean). This is consistent with the upper limit of 3.36 ± 0.10 eV ascertained in the CID experiment of $OPtO^+$ with Xe, reaction 14. Our BDE for OPt^+-O is much smaller than the value of 4.1 ± 0.4 eV obtained by combining data on PtO_2 from Knudsen cell mass spectrometry experiments[40,41] with an electron impact ionization energy (IE) of 11.2 ± 0.3 eV from the same study.[10,42] Brönstrup et al. similarly bracketed this IE as about 11.1 ± 0.6 eV.[10]

Our experimental BDE is close to the theoretical values of 2.85 (B3LYP/BS II), 2.76 (B3LYP/BS III), 3.50 (MR-QDPT/BS IV), and 3.62 (CASPT2/BS V) eV calculated by Brönstrup et al.[10] for the $OPtO^+$ species. Our own B3LYP calculations find a second bond energy of 2.64 eV, comparable to the B3LYP values from Brönstrup et al.[10] These results are summarized in Table 2. The similarity of the second and first platinum−oxygen experimental BDEs and the good agreement with theory demonstrates that the PtO_2^+ ions formed in reactions 4 and 8 have a dioxide structure. Further, if this species were formed by a simple ligand exchange process to form $Pt^+\cdot O_2$ in the reaction of $PtO^+ + O_2$, then the thermochemistry determined below and in the preceding paper[1] indicates that the threshold should correspond to 2.59 ± 0.06 eV $= D_0(Pt^+-O) - D_0(Pt^+-O_2) = 3.26-0.67$. Instead, the threshold is measured to be 2.04 ± 0.05 eV. This also implies that PtO_2^+ probably has a dioxide structure as discussed further as below. Additional evidence for such a structure comes from the observation that these PtO_2^+ species dissociate readily by O atom loss even though O_2 elimination is a lower energy channel, Figure 6.

As discussed in detail by Brönstrup et al.,[10] the characterization of the ground state of PtO_2^+ is problematic, but the most advanced multireference calculations indicate that the ground state of $O-Pt^+-O$ is $^2\Sigma_g^+$. Their B3LYP calculations find a bent species, $^2A_1$ symmetry, having a bond angle of $\sim 160°$.[10,43] Our calculations indicate that the $^2\Sigma_g^+$ state has a valence electron configuration of $1\sigma_g^2 1\sigma_u^2 2\sigma_g^2 1\pi_g^4 2\sigma_u^2 1\delta_g^4 1\pi_u^4 3\sigma_g^1$. The $1\sigma_g$ and $1\sigma_u$ orbitals are O(2s) based; the $2\sigma_g$ and $1\pi_g$ are bonding orbitals, the $2\sigma_u$ and $1\pi_u$ are nonbonding combinations of the three O(2p) orbitals, the 1δ are pure metal 5d nonbonding orbitals, and the $3\sigma_g$ is largely Pt(6s). Thus, PtO_2^+ has an electronic structure analogous to CO_2 with strong σ and π bonding. (One interesting aspect of our own B3LYP calculations on PtO_2^+ is that the lowest energy species (0.30 eV lower than the $^2\Sigma_g^+$ state) was found to be $^2\Sigma^+(A')$ with unequal Pt−O bond lengths, 1.757 and 1.780 Å, and a linear geometry, $\angle OPtO = 180.0°$. Further investigation of this symmetry breaking phenomenon would be interesting although the present result could also be an artifact of the basis set and level of theory used.) We also found a $^2A''$ state having a nonlinear geometry with unequal PtO bond lengths, Table 3, lying 1.06 eV above the $^2\Sigma^+$ ground state. The lowest quartet state of PtO_2^+ was a $^4B_2$ state, in agreement with Brönstrup et al.,[10] which we find lies 0.37 eV above the $^2\Sigma^+$ ground state, Table 3.

The sum of the Pt^+-O and OPt^+-O bond energies determined here and the preceding study, 6.32 ± 0.10 eV, means that loss of O_2 from ground-state $OPtO^+$ requires 1.20 ± 0.10 eV. This agrees with the threshold measured for this process, Table 1, 1.19 ± 0.10 eV, suggesting that reductive elimination of O_2 from the dioxide has no barrier in excess of the endothermicity of the reaction. This conclusion is discussed in more detail below in conjunction with calculations for the potential energy surface of the PtO_2^+ system.

4.3. $Pt^+\cdot O_2$. The BDE of Pt^+-O_2 is determined by CID of PtO_2^+ formed by three-body condensation of Pt^+ and O_2 with Ar and Xe. In the reactions of PtO_2^+ with Ar/Xe, only simple CID and ligand exchange channels (reactions 11 and 12) are found. The failure to observe any PtO^+ product, which is observed as a facile product from $OPtO^+$, suggests that the PtO_2^+ formed this way has the $Pt^+\cdot O_2$ structure. The CID thresholds are found to be 0.67 ± 0.05 eV for the Ar system and 0.79 ± 0.05 eV for the Xe system. Note that both values are much less than the 1.20 ± 0.10 eV energy required for O_2 loss from $OPtO^+$. Because the fitting is much better and competitive suppression of the CID channel from the ligand exchange reaction 12 is much less for the Ar system, the threshold value obtained from the Ar system should be a more accurate BDE for Pt^+-O_2.

Helping to confirm the structure of this molecule, our experimental value is found to be close to the theoretical values for the Pt^+-O_2 species of 0.65 (B3LYP/BS II), 0.65 (B3LYP/BS III), 0.77 (MR-QDPT/BS IV), and 0.89 (CASPT2/BS V) eV calculated by Brönstrup et al.,[10] after an approximate

TABLE 3: Bond Lengths (Å), Bond Angles (deg), and Energies Calculated at the B3LYP/HW+/6-311+G(3df) Level for PtO_2^+

	r(Pt−O)	r(O−O)	∠OPtO	∠PtOO	E (h)	ZPE (h)	E_{rel} (eV)[a]
$Pt^+(^2D) + O_2$		1.203			−269.116743	0.003748	0.000
$Pt^+(^4F) + O_2$		1.203			−269.091692	0.003748	0.682
$PtO^+(^4\Sigma^-) + O$	1.764				−269.038372	0.001770	2.080
$PtO^+(^2\Sigma^-) + O$	1.766				−269.028431	0.001772	2.350
$Pt^+\cdot O_2(^2A'')$	2.040	1.209		118.4	−269.152056	0.004684	−0.936
$Pt^+\cdot O_2(^4A'')$	2.121	1.208		120.5	−269.146148	0.004656	−0.776
$Pt^+\cdot O_2(^2A')$	2.070	1.204		123.3	−269.140716	0.004435	−0.634
$OPtO^+(^2\Sigma^+, {}^2A')$	1.780, 1.757		180.0		−269.137275	0.003938	−0.554
$OPtO^+(^2\Sigma_g^+)$	1.704		180.0		−269.127285	0.004933	−0.255
$OPtO^+(^4B_2)$	1.779		111.4		−269.123588	0.003875	−0.183
$OPtO^+(^2A'')$	1.763, 1.818		112.1		−269.097691	0.003346	0.508
$OPtO^+(^4A_1)$	1.871		66.5		−269.079899	0.003555	0.997
$OPtO^+(^4A_1)$ TS[b]	1.927		52.3		−269.062304	0.002546	1.449
$OPtO^+(^2A'')$ TS[b]	1.826, 1.970		60.8		−269.060132	0.002690	1.512
$OPtO^+(^2A')$ TS[b]	1.884, 1.932		52.8		−269.047705	0.002080	1.834
$OPtO^+(^4B_1)$ TS[b]	1.919		54.7		−269.041153	0.002750	2.030

[a] Energies relative to the $Pt^+(^2D) + O_2$ asymptote including corrections for zero-point energies (ZPE) scaled by 0.9804. These energies do not include the 0.418 eV correction for the spin−orbit levels of $Pt^+(^2D)$. [b] TS = transition state.

correction of 0.418 eV for Pt^+ spin−orbit asymptote as explained in the preceding paper.[1,20,44] Our B3LYP calculations find a ground-state bond energy of 0.52 eV, Table 2. The associative PtO_2^+ has a $^2A''$ ground-state according to theoretical calculations.[10] This species has an end-on peroxide structure (∠PtOO = 107° for the multireference calculations, ∼118° for the B3LYP calculations).[10] We also find a $^2A''$ ground state with $^4A''$ and $^2A'$ states lying 0.16 and 0.30 eV higher in energy, respectively. Geometries and energies for these species are given in Table 3.

4.4. OPt^+−CO. $PtCO_2^+$ is observed as a product in the reaction of PtO^+ with CO_2. If this species were formed by a simple ligand exchange process to form $Pt^+(CO_2)$, then the thermochemistry determined in the preceding paper[1] indicates that the threshold should correspond to 2.64 ± 0.06 eV = $D_0(Pt^+-O) - D_0(Pt^+-CO_2) = 3.26-0.62$. Instead, the threshold is measured to be 3.24 ± 0.10 eV. If we assume that the structure of this complex is OPt^+−CO, then this threshold yields a bond energy of $D_0(OPt^+-CO) = 2.21 \pm 0.10$ eV, similar to the bond energy of Pt^+−CO, 2.26 ± 0.09 eV.[1,21] Given this structural assignment, we can also calculate that the bond energy of $OCPt^+$−O is 3.21 ± 0.12 eV, which is comparable with $D_0(Pt^+-O) = 3.26 \pm 0.07$ eV.[1] The similarity of the Pt^+−CO/OPt^+−CO and Pt^+−O/$OCPt^+$−O bond energies is certainly consistent with the OPt^+−CO structure. Our calculations indicate that the inserted $OPtCO^+$ species has several stable minima, as described fully in the preceding paper.[1] The ground state is calculated to be $^4\Sigma^-$ with bond energies of $D_0(OPt^+-CO) = 1.90$ eV and $D_0(OCPt^+-O) = 2.41$ eV. These values are somewhat smaller than the calculated values of $D_0(Pt^+-CO) = 2.27$ eV and $D_0(Pt^+-O) = 2.78$ eV. Note that all theoretical values are below the experimental values.

4.5. Pt^+−Ar. In the ligand exchange process of PtO_2^+ with Ar, the threshold of 0.29 ± 0.05 eV for production of $PtAr^+$ should equal the difference in BDEs for Pt^+-O_2 and Pt^+−Ar. This gives a BDE of 0.38 ± 0.07 eV for Pt^+−Ar. Similarly a BDE of 0.30 ± 0.07 eV for Pt^+−Ar is obtained from the ligand exchange process of $PtCO_2^+$ with Ar in the preceding paper.[1] A weighted average of the two values for the bond energy of Pt^+−Ar is 0.34 ± 0.09 eV (two standard deviations of the mean). This is comparable to BDEs of Mg^+−Ar at 0.10 ± 0.07 eV,[45] V^+−Ar at 0.2 ± 0.2 eV,[46] Fe^+−Ar at 0.11 ± 0.08 eV,[39] Li^+−Ar at 0.34 ± 0.14 eV,[47] Na^+−Ar at 0.16 ± 0.09 eV,[47] and K^+−Ar at 0.19 ± 0.07 eV.[47]

4.6. Pt^+−Xe. $PtXe^+$ is observed in the reactions of PtO_2^+ with Xe and, as reported in the previous paper,[1] of $PtCO_2^+$ with Xe. Both of these ligand exchange reactions are found to be exothermic. These results indicate that $D_0(Pt^+-Xe)$ is greater than $D_0(Pt^+-O_2) = 0.67 \pm 0.05$ eV and $D_0(Pt^+-CO_2) = 0.62 \pm 0.05$ eV. This is consistent with the BDE of 0.86 ± 0.30 eV for Pt^+−Xe determined in other experiments.[20,21]

5. Discussion

5.1. Ionization Energy of PtO_2. The bond energies and ionization energies of platinum monoxide and platinum dioxide can be related according to the thermochemical cycle, D(OM−O) + IE(MO) = D(OM^+−O) + IE(MO_2). The neutral OPt−O BDE has been measured as 4.1 ± 0.4 eV using the mass spectrometric Knudsen cell method.[40] Thus, given IE(PtO) = 9.52 ± 0.25 eV[1] and the OPt^+−O BDE measured here, we can calculate that IE(PtO_2) is 10.56 ± 0.48 eV. This is close to the lower limit for IE(PtO_2) of 11.2 ± 0.3 eV determined by electron impact studies in the early literature[40] and falls within the bracket of 11.1 ± 0.6 eV determined by Brönstrup et al.[10] Indeed, these authors found that PtO_2^+ undergoes charge transfer with ethene (IE = 10.5 eV), accounting for about 40% of the products, behavior consistent with the value of IE(PtO_2) determined here. Thus, ionization of PtO_2 reduces the bond strength (or equivalently, oxidation raises the ionization energy) by 1.0 ± 0.4 eV, an effect similar to that found for the PtO species.[1]

As noted above, the ground state of $OPtO^+$ is $^2\Sigma_g^+$ with an electron configuration of $1\sigma_g^2 1\sigma_u^2 2\sigma_g^2 1\pi_g^4 2\sigma_u^2 1\delta_g^4 1\pi_u^4 3\sigma_g^1$. From this, we can speculate that OPtO has a $^1\Sigma_g^+$ ground state with an electron configuration of $1\sigma_g^2 1\sigma_u^2 2\sigma_g^2 1\pi_g^4 2\sigma_u^2 1\delta_g^4 1\pi_u^4 3\sigma_g^2$. The observation that the Pt−O bond energy decreases upon ionization suggests that the $3\sigma_g$ orbital has bonding character, which indicates that this orbital must contain some O($2p\sigma$) character in addition to the dominant Pt(6s) contribution.

5.2. Excited States of PtO^+. In the reaction of $PtO^+ + O_2$, there is a small tail in the PtO_2^+ cross section at lower energies (visible in the expansion of the data, Figure 2) that probably results from trace amounts of excited states of the PtO^+ reactant, as identified in the previous paper for the reaction of PtO^+ with CO.[1] However, the presence of the excited states in the latter reaction is much more evident than in the $PtO^+ + O_2$ reaction. We believe this may have to do with the details of the potential energy surfaces in the two systems. The reaction of ground-state $PtO^+(^4\Sigma^-)$ with $O_2(^3\Sigma_g^-)$ to form $PtO_2^+(^2\Sigma^+) + O(^3P)$ can occur easily along a doublet potential energy surface, thus involving covalent bond formation from both reactants and products. Likewise, the reaction of excited-state $PtO^+(^2\Sigma^-)$ with

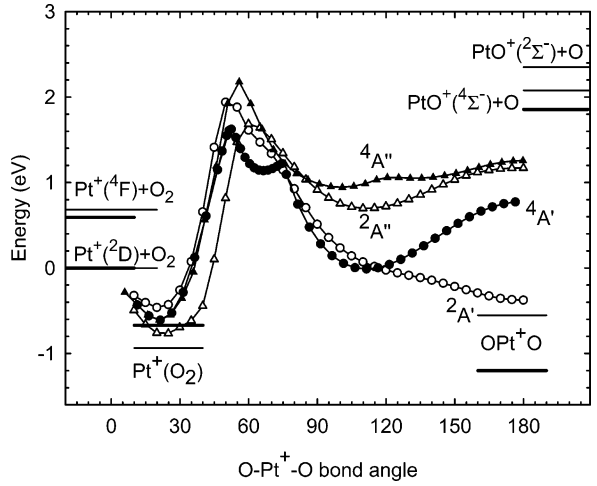

Figure 7. Relaxed potential energy surface scans of the bond angle for the PtO_2^+ system calculated at the B3LYP/HW+/6-31+G(2d) level. Circles and triangles represent surfaces of A′ and A″ symmetry, respectively. Open and closed symbols represent doublet and quartet surfaces, respectively. Calculated energies of reactant and product asymptotes with a larger basis set (see text) are indicated by horizontal bars to the left and right, respectively. Thicker horizontal bars indicate experimental energies of reactants, intermediates, and products.

$O_2(^3\Sigma_g^-)$ leading to $PtO_2^+(^2\Sigma^+) + O(^3P)$ is also spin-allowed and can occur along a doublet surface. Thus, the excited states presumably contribute little to the observed PtO_2^+ cross section (Figure 2) because their population is relatively low. This conclusion is consistent with the failure to observe obvious contributions from the excited state of PtO^+ in the cross sections for the CID of PtO^+ with Xe and the reaction of PtO^+ with CO_2. In contrast, as discussed in detail in the previous article,[1] the dynamics for the production of $PtCO^+ + O$ is facile in the reaction of CO with the $PtO^+(^2\Sigma^-)$ excited state, but the collinear approach required for the reaction involving the $PtO^+(^4\Sigma^-)$ ground state inhibits this channel. Thus, the presence of the excited states is much more evident in this reaction system.

5.3. Potential Energy Surfaces and Reaction Mechanisms. Combined with the study of the $Pt^+ + O_2$ reaction in the preceding paper,[1] our experiments can probe the potential energy surfaces for the activation of O_2 by Pt^+ by independently starting at three separate places on the same global surface, i.e., reactants, intermediates, and products. This potential energy surface (PES) can be constructed as follows from the various bond energies measured here and compared with calculations, as shown in Figure 7. As noted above, the surfaces calculated used a double-ζ basis set on oxygen, such that the energies are not as accurate as those listed in Table 3. As discussed in detail by Brönstrup et al.,[10] the relative energies of the $Pt^+\cdot O_2$ and $OPtO^+$ species are not predicted well at such a level, nor is the absolute energy of the dioxide. Nevertheless, the qualitative features of this PES may be useful in providing insight into the PtO_2^+ system. To facilitate the comparison between these calculations and experimental results, the 0.418 eV correction for the spin−orbit states of Pt^+ is ignored in Figure 7.

For the activation of $O_2(^3\Sigma_g^-)$ by $Pt^+(^2D)$, the first step is to form a $Pt^+\cdot O_2(^2A'')$ intermediate at -0.67 ± 0.05 eV. Clearly, formation of such adducts in $^2A'$, $^4A'$, and $^4A''$ states is also possible as the ground-state reagents can combine to form five doublet and five quartet surfaces. These associative $Pt^+\cdot O_2$ complexes may then pass over an energy barrier to form the platinum dioxide cation in a number of different states. Ground-state $O-Pt^+-O(^2\Sigma^+)$ with an experimental energy of -1.20 ± 0.10 eV relative to the $Pt^+ + O_2$ entrance channel is formed along the $^2A'$ surface. This surface has a higher barrier than other surfaces, but one that is calculated to lie 0.25 eV below the $PtO^+(^4\Sigma^-) + O(^3P)$ products, which have an experimental endothermicity of 1.85 ± 0.07 eV relative to the $Pt^+(^2D) + O_2(^3\Sigma_g^-)$ entrance channel. The $^2A''$ surface has a lower barrier, calculated to lie 0.57 eV below the products. Likewise on the $^4A'$ and $^4A''$ surfaces, the TSs (having $^4A_1$ and $^4B_1$ symmetries, respectively, Table 3) are found to lie 0.63 and 0.05 eV, respectively, below the products. The observation that the threshold for formation of PtO^+ is consistent with the thermochemistry determined in other systems indicates that there are no barriers in excess of the endothermicity of the reaction, consistent with the qualitative character of the PESs shown in Figure 7. On the basis of the dissociation behavior observed for $Pt^+\cdot O_2$ and $O-Pt^+-O$, it seems most likely that the $PtO^+ + O$ products are formed from $O-Pt^+-O$ by cleavage of the Pt−O bond.

The surfaces shown in Figure 7 make it clear why the dissociation behavior of PtO_2^+ formed by association of Pt^+ with O_2 and by sequential reactions with N_2O differs. The former method of ion generation produces $Pt^+\cdot O_2$ which can readily exchange the O_2 ligand for a rare gas collision partner or dissociate by losing the O_2 ligand at low energies. Loss of an oxygen atom requires surmounting the tight transition state associated with insertion into the O_2 bond such that this pathway is not competitive. In contrast, the latter method of ion generation forms the $O-Pt^+-O$ dioxide, which can readily lose an oxygen atom once this pathway is energetically available. At lower energies, the dioxide can also rearrange to reductively eliminate O_2 by passing over the tight transition state. Experimentally, the threshold for this process equals the thermodynamic value for production of $Pt^+ + O_2$, whereas the theoretical surfaces indicate that there are substantial barriers above $Pt^+ + O_2$. Apparently, this is another reflection of the difficulty that theory (especially at the B3LYP level) has in accurately describing the PtO_2^+ system. As discussed in detail by Brönstrup et al.,[10] this is largely because of the multireference character of PtO_2^+, a problem that seems likely to be even more severe for the TSs. We reject an alternative explanation for a low threshold for O_2 elimination that involves PtO_2^+ ions having excess internal energy. This seems unlikely because the energy threshold for production of PtO^+ is consistent with the thermodynamic BDE for PtO_2^+ from the other experiments. As both dissociations are spin-allowed, they should both be sensitive to such excitation. Because the O_2 elimination channel involves a tight transition state compared to the loose transition state for O atom elimination, competition between these two pathways is evident in the data, Figure 6. Evidence for a barrier between the $Pt^+\cdot O_2$ adduct and the $O-Pt^+-O$ dioxide structures has also been found in the related neutral system. There, reaction of $Pt + O_2$ leads to formation of a $Pt\cdot O_2$ adduct, which converts to platinum dioxide under photolysis.[48−50]

For the reactions of PtO^+ with O_2, one again imagines that an associative complex with a peroxide structure, $OPt^+\cdot O_2$, can be formed. Formation of $O-Pt^+-O(^2\Sigma^+) + O(^3P)$ products, which has an endothermicity of 2.06 ± 0.07 eV relative to the entrance channel of $PtO^+(^4\Sigma^-) + O_2(^3\Sigma_g^-)$, could occur by cleavage of the O−O bond, although the possibility of a trioxide intermediate cannot be discounted given the high spin states of the platinum oxides. The reaction $PtO^+(^4\Sigma^-) + O_2(^3\Sigma_g^-) \rightarrow PtO_2^+(^2\Sigma^+) + O(^3P)$ is spin-allowed. For the production of $Pt^+(^2D) + O(^3P) + O_2(^3\Sigma_g^-)$, a simple CID process, the reaction is also spin-allowed and is observed to begin close to the expected thermodynamic threshold.

For the reactions of PtO^+ with CO_2, the first step is probably to form an associative complex with an end-on structure for $OPt^+ \cdot OCO$. The formation of $O-Pt^+-O(^2\Sigma^+) + CO(^1\Sigma^+)$ products has an endothermicity of 2.40 ± 0.05 eV relative to the entrance channel of $PtO^+(^4\Sigma^-) + CO_2(^1\Sigma_g^+)$. As noted above, the $PtCO_2^+$ species formed in this reaction appears to have a OPt^+-CO structure, which indicates that the CO_2 bond has been activated, suggesting that a $(O)_2Pt^+-CO$ intermediate is probably formed. Clearly, this species can dissociate by loss of CO to form $OPtO^+$ or by loss of O to yield $OPtCO^+$. The agreement of the thresholds measured here with other thermodynamic information indicates that there are no barriers along the reaction path in excess of the endothermicity for PtO_2^+ or $OPtCO^+$ formation. For the production of $Pt^+ + O + CO_2$, a simple CID process, the measured endothermicity is near that expected from the Pt^+-O BDE measured in the other systems.

6. Conclusion

Guided ion beam tandem mass spectrometry is used to characterize the kinetic energy dependences of the reactions of PtO^+ with O_2 and CO_2, collision-induced dissociation of PtO^+ with Xe and PtO_2^+ with Xe and Ar. Analysis of endothermic reaction cross sections leads to 0 K bond dissociation energies for OPt^+-O, Pt^+-O_2, OPt^+-CO, and Pt^+-Ar, which are reasonably consistent with available theoretical values. These results along with theoretical calculations are used to construct potential energy surfaces for the activation of O_2 by Pt^+, which help elucidate the reaction mechanisms. These results indicate that this reaction proceeds via an insertion mechanism, and this seems likely for the activation of O_2 and CO_2 by PtO^+ as well.

Acknowledgment. This work was supported by the National Science Foundation under Grant CHE-0135517. The authors thank J. N. Harvey and D. Schröder for supplying details about their calculations of Pt^+-O_2 and OPt^+-O.

References and Notes

(1) Zhang, X.-G.; Armentrout, P. B. *J. Phys. Chem. A*, **2003**, *107*, 8904. in this issue.
(2) Somorjai, G. A. *Introduction to Surface Chemistry and Catalysis*; Wiley: New York, 1994.
(3) Crabtree, R. H. *The Organometallic Chemistry of the Transition Metals*, 2nd ed.; Wiley: New York, 1994.
(4) Clemmer, D. E.; Dalleska, N. F.; Armentrout, P. B. *Chem. Phys. Lett.* **1992**, *190*, 259.
(5) Sievers, M. R.; Armentrout, P. B. *J. Chem. Phys.* **1995**, *102*, 754.
(6) Sievers, M. R.; Armentrout, P. B. *Int. J. Mass Spectrom.* **1998**, *179−180*, 103.
(7) Sievers, M. R.; Armentrout, P. B. *J. Phys. Chem. A* **1998**, *102*, 10754.
(8) Sievers, M. R.; Armentrout, P. B. *Inorg. Chem.* **1999**, *38*, 397.
(9) Sievers, M. R.; Armentrout, P. B. *Int. J. Mass Spectrom.* **1999**, *185−187*, 117.
(10) Brönstrup, M.; Schröder, D.; Kretzschmar, I.; Schwarz, H.; Harvey, J. N. *J. Am. Chem. Soc.* **2001**, *123*, 142.
(11) Wesendrup, R.; Schröder, D.; Schwarz, H. *Angew. Chem., Int. Ed. Engl.* **1994**, *33*, 1174.
(12) Pavlov, M.; Blomberg, M. R. A.; Siegbahn, P. E. M.; Wesendrup, R.; Heinemann, C.; Schwarz, H. *J. Phys. Chem. A* **1997**, *101*, 1567.
(13) Schröder, D.; Schwarz, H. *Angew. Chem., Int. Ed. Engl.* **1995**, *34*, 1973.
(14) Armentrout, P. B.; Kickel, B. L. In *Organometallic Ion Chemistry*; Freiser, B. S., Ed.; Kluwer: Dordrecht, 1996; p 1.
(15) Armentrout, P. B. In *Topics in Organometallic Chemistry*; Brown, J. M., Hofmann, P., Eds.; Springer-Verlag: Berlin, 1999; Vol. 4-I, p 1.
(16) Kretzschmar, I.; Schröder, D.; Schwarz, H.; Armentrout, P. B. *Adv. Met., Semicond. Clusters* **2001**, *5*, 347.
(17) Loh, S. K.; Hales, D. A.; Lian, L.; Armentrout, P. B. *J. Chem. Phys.* **1989**, *90*, 5466.
(18) Schultz, R. H.; Armentrout, P. B. *Int. J. Mass Spectrom. Ion Processess* **1991**, *107*, 29.
(19) Armentrout, P. B. *Int. J. Mass Spectrom.* **2000**, *200*, 219.
(20) Zhang, X.-G.; Liyanage, R.; Armentrout, P. B. *J. Am. Chem. Soc.* **2001**, *123*, 5563.
(21) Zhang, X.-G.; Armentrout, P. B. *Organometallics* **2001**, *20*, 4266.
(22) Chesnavich, W. J.; Bowers, M. T. *J. Phys. Chem.* **1979**, *83*, 900.
(23) Armentrout, P. B. In *Advances in Gas-Phase Ion Chemistry*; Adams, N. G., Babcock, L. M., Eds.; JAI: Greenwich, 1992; Vol. 1, p 83.
(24) Muntean, F.; Armentrout, P. B. *J. Chem. Phys.* **2001**, *115*, 1213.
(25) Huber, K. P.; Herzberg, G. *Molecular Spectra and Molecular Structure*, IV; Constants of Diatomic Molecules; Van Nostrand Reinhold: New York, 1979.
(26) Shimanouchi, T. *Tables of Molecular Vibrational Frequencies*, Consolidated Vol. I, NSRDS-NBS *39*, 1972.
(27) The vibrational frequency of PtO^+ is taken from the theoretical value of 799 cm^{-1} (ref 10).
(28) Ervin, K. M.; Armentrout, P. B. *J. Chem. Phys.* **1985**, *83*, 166.
(29) Weber, M. E.; Elkind, J. L.; Armentrout, P. B. *J. Chem. Phys.* **1986**, *84*, 1521.
(30) Becke, A. D. *J. Chem. Phys.* **1993**, *98*, 5648.
(31) Lee, C.; Yang, W.; Parr, R. G. *Phys. Rev. B* **1988**, *37*, 785.
(32) Frisch, M. J.; Trucks, G. W.; Schlegel, H. B.; Scuseria, G. E.; Robb, M. A.; Cheeseman, J. R.; Zakrzewski, V. G.; Montgomery, J. A., Jr.; Stratmann, R. E.; Burant, J. C.; Dapprich, S.; Millam, J. M.; Daniels, A. D.; Kudin, K. N.; Strain, M. C.; Farkas, O.; Tomasi, J.; Barone, V.; Cossi, M.; Cammi, R.; Mennucci, B.; Pomelli, C.; Adamo, C.; Clifford, S.; Ochterski, J.; Petersson, G. A.; Ayala, P. Y.; Cui, Q.; Morokuma, K.; Malick, D. K.; Rabuck, A. D.; Raghavachari, K.; Foresman, J. B.; Cioslowski, J.; Ortiz, J. V.; Baboul, A. G.; Stefanov, B. B.; Liu, G.; Liashenko, A.; Piskorz, P.; Komaromi, I.; Gomperts, R.; Martin, R. L.; Fox, D. J.; Keith, T.; Al-Laham, M. A.; Peng, C. Y.; Nanayakkara, A.; Gonzalez, C.; Challacombe, M.; Gill, P. M. W.; Johnson, B.; Chen, W.; Wong, M. W.; Andres, J. L.; Gonzalez, C.; Head-Gordon, M.; Replogle, E. S.; Pople, J. A. *Gaussian 98*, Revision A.11; Gaussian, Inc.: Pittsburgh, PA, 1998.
(33) Ohanessian, G.; Brusich, M. J.; Goddard, W. A., III. *J. Am. Chem. Soc.* **1990**, *112*, 7179.
(34) Hay, P. J.; Wadt, W. R. *J. Chem. Phys.* **1985**, *82*, 299.
(35) Foresman, J. B.; Frisch, A. E. *Exploring Chemistry with Electronic Structure Methods*; Gaussian, Inc.: Pittsburgh, 1996.
(36) Armentrout, P. B.; Simons, J. *J. Am. Chem. Soc.* **1992**, *114*, 8627.
(37) Sievers, M. R.; Chen, Y.-M.; Armentrout, P. B. *J. Chem. Phys.* **1996**, *105*, 6322.
(38) Andersen, A.; Muntean, F.; Walter, D.; Rue, C.; Armentrout, P. B. *J. Phys. Chem. A* **2000**, *104*, 692.
(39) Tjelta, B. L.; Walter, D.; Armentrout P. B. *Int. J. Mass Spectrom.* **2001**, *204*, 7.
(40) Norman, J. H.; Staley, H. G.; Bell, W. E. *J. Phys. Chem.* **1967**, *71*, 3686.
(41) Norman, J. H.; Staley, H. G.; Bell, W. E. *Adv. Chem. Ser.* **1968**, *71*, 101.
(42) Lias, S. G.; Bartmess, J. E.; Liebman, J. F.; Holmes, J. L.; Levin, R. D.; Mallard, W. G. *J. Phys. Chem. Ref. Data, Suppl. 1*, **1988**.
(43) Harvey, J. N. Personal communication.
(44) Zhang, X.-G.; Armentrout, P. B. *J. Chem. Phys.* **2002**, *116*, 5565.
(45) Andersen, A.; Muntean, F.; Walter, D.; Rue, C.; Armentrout, P. B. *J. Phys. Chem. A* **2000**, *104*, 692.
(46) Aristov, N.; Armentrout, P. B. *J. Phys. Chem.* **1986**, *90*, 5135.
(47) Walter, D.; Sievers, M. R.; Armentrout, P. B. *Int. J. Mass Spectrom. Ion Processes* **1998**, *175*, 93.
(48) Bare, W. D.; Citra, A.; Chertihin, G. V.; Andrews, L. *J. Phys. Chem. A* **1999**, *103*, 5456.
(49) Wang, X.; Andrews, L. *J. Phys. Chem. A* **2001**, *105*, 5812.
(50) Danset, D.; Manceron, L.; Andrews, L. *J. Phys. Chem. A* **2001**, *105*, 7205.